Nucleosome Positioning by an Evolutionarily Conserved Chromatin Remodeler Prevents Aberrant DNA Methylation in *Neurospora*

Andrew D. Klocko,*[,1,2] Miki Uesaka,[†] Tereza Ormsby,*[,3] Michael R. Rountree,*[,4] Elizabeth T. Wiles,* Keyur K. Adhvaryu,* Shinji Honda,[†] and Eric U. Selker*[,2]

*Institute of Molecular Biology, University of Oregon, Eugene, Oregon 97403 and [†]Faculty of Medical Sciences, University of Fukui, 910-1193, Japan

ORCID IDs: 0000-0002-2236-672X (A.D.K.); 0000-0002-2953-9208 (T.O.); 0000-0003-2371-6389 (M.R.R.); 0000-0001-6465-0094 (E.U.S.)

ABSTRACT In the filamentous fungus *Neurospora crassa*, constitutive heterochromatin is marked by tri-methylation of histone H3 lysine 9 (H3K9me3) and DNA methylation. We identified mutations in the *Neurospora* defective in methylation-1 (*dim-1*) gene that cause defects in cytosine methylation and implicate a putative AAA-ATPase chromatin remodeler. Although it was well-established that chromatin remodelers can affect transcription by influencing DNA accessibility with nucleosomes, little was known about the role of remodelers on chromatin that is normally not transcribed, including regions of constitutive heterochromatin. We found that *dim-1* mutants display both reduced DNA methylation in heterochromatic regions as well as increased DNA methylation and H3K9me3 in some intergenic regions associated with highly expressed genes. Deletion of *dim-1* leads to atypically spaced nucleosomes throughout the genome and numerous changes in gene expression. DIM-1 localizes to both heterochromatin and intergenic regions that become hyper-methylated in *dim-1* strains. Our findings indicate that DIM-1 normally positions nucleosomes in both heterochromatin and euchromatin and that the standard arrangement and density of nucleosomes is required for the proper function of heterochromatin machinery.

KEYWORDS heterochromatin; DIM-1; CATP; nucleosome; DNA methylation; *Neurospora crassa*

NUCLEOSOMES do more than compact DNA. The arrangement of nucleosomes and the post-translational modifications of their constituent histones serve regulatory mechanisms, *e.g.*, to regulate cellular responses to environmental and developmental stimuli through transcriptional control (Vermaak and Wolffe 1998; Clapier and Cairns 2009; Henikoff 2016; Lai and Pugh 2017; Lämke and Bäurle 2017). Conserved chromatin remodelers have been identified that place, remove, or shift nucleosomes on DNA, and that can elicit a cascade of defects if compromised (Soppe *et al.* 2002; Tsukiyama 2002; Henikoff 2016; Clapier *et al.* 2017; Hammond *et al.* 2017; Lai and Pugh 2017). Despite advances identifying and characterizing the role of chromatin remodelers in gene expression, much remains to be learned about how they work (Tsukiyama 2002). Moreover, a major gap in our knowledge concerns possible effects of nucleosome positioning on heterochromatin, which is the largely silent fraction of the genome (Grewal and Jia 2007; Rountree and Selker 2010; Allshire and Madhani 2017). Constitutive heterochromatin is mostly in centromeric regions, and is gene-poor, rich in repeated sequences, generally marked by methylation of lysine 9 of histone H3 (H3K9me) and cytosine methylation, and contains characteristic proteins such as Heterochromatin Protein-1 (HP1) (Henikoff 2000; Freitag *et al.* 2004; Grewal and Jia 2007; Lewis *et al.* 2008; Bühler and Gasser 2009; Freitag 2017). This form of heterochromatin is responsible for silencing transcription and recombination

doi: https://doi.org/10.1534/genetics.118.301711
Manuscript received October 17, 2018; accepted for publication December 11, 2018; published Early Online December 14, 2018.
Supplemental material available at Figshare: https://doi.org/10.25386/genetics.7210190.
[1]Present address: Department of Chemistry and Biochemistry, University of Colorado Colorado Springs, 1420 Austin Bluffs Parkway, Colorado Springs, CO 80918.
[2]Corresponding authors: University of Oregon, 1370 Franklin Blvd., Eugene, OR 97403. E-mail: selker@uoregon.edu; and aklocko@uccs.edu
[3]Present address: Department of Biochemistry, Faculty of Science, Charles University, Hlavova 2030, 128 00 Prague 2, Czech Republic.
[4]Present address: Nzumbe Inc., 3439 NE Sandy Blvd. #330, Portland, OR 97232.

of underlying selfish DNA, and plays roles in chromosome segregation and genome organization (Henikoff 2000; Lewis *et al.* 2008). Facultative heterochromatin is also transcriptionally quiescent but is associated with functional genes and its distribution can change during development and/or as a result of environmental changes. In most eukaryotes, facultative heterochromatin is marked by methylation of lysine 27 of histone H3 (H3K27me) (Trojer and Reinberg 2007; Wutz 2011; Connolly *et al.* 2013; Jamieson *et al.* 2013; Freitag 2017; Wiles and Selker 2017). Changes in heterochromatin have been associated with developmental defects, cancer, and embryonic lethality (Ronemus *et al.* 1996; Okano *et al.* 1999; Tachibana *et al.* 2002; Heard 2005; Wutz 2011; Connolly *et al.* 2013; Elgin and Reuter 2013; Lewis and Allis 2013; Lewis *et al.* 2013; Timp and Feinberg 2013; Grossniklaus and Paro 2014; Morgan and Shilatifard 2015; Studt *et al.* 2016).

Information on the genes necessary for the formation and regulation of heterochromatin is limited, prompting investigations in favorable model organisms with genomic features similar to higher metazoans, such as *Drosophila melanogaster* and the filamentous fungus *Neurospora crassa* (Rountree and Selker 2010; Elgin and Reuter 2013). Heterochromatin is not essential in *Neurospora*, which allows for the identification of genes involved in heterochromatin formation and function (Foss *et al.* 1993; Lewis *et al.* 2010a,b), including the Defective In Methylation-5 (DIM-5) H3K9 methyltransferase (MTase), and other members of DCDC (DIM-5/-7/-9, CUL4, DDB1$^{dim\text{-}8}$ Complex). All components of DCDC are required for H3K9me3 and localization of HP1, which specifically binds to the H3K9me3 mark (Nielsen *et al.* 2002; Freitag *et al.* 2004; Lewis *et al.* 2010a,b; Honda *et al.* 2012). HP1 directly recruits the DNA MTase DIM-2 and an HDAC complex, HCHC (HP1/CDP-2/HDA-1/CHAP), to constitutive heterochromatin and is also involved in the DMM complex, which limits spreading of heterochromatin (Honda and Selker 2008; Honda *et al.* 2010, 2012).

We report the identification and characterization of the *Neurospora dim-1* gene, which was originally found because mutations of this gene conferred resistance to the toxicity of 5-azacytidine (5-azaC) in the mutagen-sensitive *mus-20* genetic background; the mutant was also found to be partially defective in DNA methylation. We identified the gene, showed that it encodes an AAA-ATPase nucleosome remodeler conserved from yeast to humans, and found that a strain with a deletion of the gene (Δ*dim-1*) has altered nucleosome positions throughout the genome. Loss of DIM-1 causes constitutive heterochromatin to lose much of its cytosine methylation although the underlying H3K9me3 is retained. In addition, intergenic regions exhibit DNA hyper-methylation in *dim-1* strains. DIM-1 and the heterochromatin machinery preferentially localize to regions of aberrant hyper-methylation, suggesting that they are targets for DIM-1 activity. We note that these regions have variable and often increased nucleosome density that mirror the nucleosome profile in heterochromatic regions and suggest that nucleosome disorder may lead to the hyper-methylation.

Materials and Methods

N. crassa strains were grown, maintained, and crossed following standard protocols (Davis 2000); strains are listed in Supplemental Material, Table S1. Gene replacement constructs and *his-3* targeting constructs were generated as described (Honda and Selker 2009) using oligonucleotides listed in Table S2. Deletion strains were obtained from the *Neurospora* knockout collection (Colot *et al.* 2006) stored at the Fungal Genetics Stock Center or remade (Δ*dim-1*::*nat1*) with the oligonucleotides listed in Table S2 using a similar protocol.

Whole-genome sequencing of *dim-1* strains [N654 (heterokaryotic strain) and N1072 (microconidiated, homokaryotic strain)] and a parental strain (N200) was performed with the Nextera kit (Illumina) following the manufacturer's protocol. Single nucleotide polymorphisms (SNPs) in parental and *dim-1* strains, relative to the *Neurospora* version 10 genome, were identified using Freebayes (https://github.com/ekg/freebayes), SNPs common between output vcf files were removed using vcf-isec in VCFtools (Danecek *et al.* 2011), genic mutations were identified using SnpEFF (Cingolani *et al.* 2012), and SNPs residing on Linkage Group III were filtered using SnpSift (Cingolani *et al.* 2012).

Bisulfite-sequencing was performed as described (Klocko *et al.* 2015; Honda *et al.* 2016) and chromatin immunoprecipitation (ChIP)-sequencing was performed as described in Jamieson *et al.* (2013); one replicate of WT H3K9me3 and the WT H3K27me2me3 data set were previously reported (NCBI GEO GSE68897) (Jamieson *et al.* 2016). All reads were mapped to the corrected (Galazka *et al.* 2016) *Neurospora* genome, version 12 (NC12), and final TDF files were generated across 25 bp windows. To generate ChIP-sequencing and bisulfite-sequencing average enrichment profiles, .bam files were uploaded to the Galaxy web platform public server at usegalaxy.org (Afgan *et al.* 2018), and the DeepTools program was used (Ramírez *et al.* 2016). Peaks of ChIP-sequencing enrichment were called with MACS2 (Zhang *et al.* 2008) or SICER (Xu *et al.* 2014) using the default settings of each program; SICER detected 119 new peaks while MACS detected 394 new peaks, and while many peaks were in agreement between the two peak call output files, differences may reflect differences in how enrichment over background is calculated or changes in the gaps between called peaks. Peak call output files for each strain and the differences between strains are provided in File S2 in a format so these data can be easily made into bed files for genome browser display. PolyA messenger RNA (mRNA)-sequencing was performed as described (Klocko *et al.* 2016), using the wild-type (WT) polyA mRNA data set as a control [GSE82222; previously published in Klocko *et al.* (2016)]; for mRNA-sequencing analysis, a $\log_2 \geq 2.0$ and $\log_2 \leq -2.0$ cut-off with adjusted *P*-values of 0.05 were used. ChIP-sequencing enriched peaks, bisulfite-sequencing methylated regions, genes with significant expression changes in Δ*dim-1*, and genes with cytosine methylation peaks that

change expression are provided in File S2. All individual locus pictures were visualized and generated on Integrative Genomics Viewer (Robinson *et al.* 2011). Southern blotting was performed as in Miao *et al.* (2000) with the denoted probe DNA (oligos listed in Table S2). Histone isolation was performed as in Honda and Selker (2009). Western blotting was performed as in Adhvaryu *et al.* (2011). Mass spectrometry was performed as in Honda *et al.* (2012). Micrococcal nuclease (MNase) digestion followed by sequencing (MNase-seq) was performed as follows. Isolated nuclei were used for input DNA; nuclei were isolated following the protocol from Klocko *et al.* (2015). Frozen nuclei in storage buffer were thawed and resuspended in MNase digestion buffer [10 mM Hepes-NaOH, pH 7.5, 10 mM KCl, 1.5 mM $MgCl_2$, 50 μg/ml filter-sterilized bovine serum albumin, β-mercaptoethanol 5 mM final)] and pepstatin (10 μg/ml final), leupeptin (10 μg/ml final), and PMSF (1 mM final) were added before use. DNA concentration was determined by removing a 10 μl fraction, adding SDS to 1% to solubilize nuclear membranes and DNA quantified with a Qubit HS in triplicate. Nuclei containing 16 μg of DNA were adjusted to 400 μl with MNase digestion buffer, $CaCl_2$ was added to a final concentration of 2 mM, MNase (New England Biolabs, Beverly, MA) was added to a final concentration of 0.5 unit/μl, and the reaction was carried out at 37° for 20 min. At 2-min intervals, 30 μl aliquots (corresponding to 1.2 μg of DNA) were removed and mixed with 8 μl of 100 mM EGTA to stop the reaction and stored on ice. RNase A (5 μg) was then added to all samples and they were incubated an additional 10 min at 37° before addition of SDS to a final concentration of 1% to solubilize the nuclear membranes. DNA was purified from samples with a Qiagen MinElute Kit, and either used for Southern blotting or sequencing. For MNase-seq, the mono- and di-nucleosome populations, with the associated linker DNA, of two independent biological replicates of the 8- and 10-min samples were pooled for sequencing, reasoning that at earlier time points, the slower-digested euchromatic regions and the rapidly digested heterochromatic regions would be present in our data. While mono- and di-nucleosome populations were analyzed (independently and combined), for simplicity, only data from mono-nucleosomes are shown in the figures. MNase-sequencing libraries were constructed using the Illumina TruSeq kit, following the manufacturer's protocols with the following modifications. After end repair, DNA was purified using a Qiagen MinElute Kit, as recommended by Lombardi *et al.* (2014). Libraries containing mono- and di-nucleosomes (and the fragments between these prominent bands) were size-selected with 2% TAE gel electrophoresis following an eight-cycle PCR amplification step; the average size of mono-nucleosomes was ~270 bp, while the average size of di-nucleosomes was ~490 bp. Libraries were sequenced on a NextSeq 500 (University of Oregon Genomics Core Facility) as 37 nt paired-end (PE) reads. Reads denoting mono-nucleosomes were mapped to the corrected *Neurospora* genome version 12 (Galazka *et al.* 2016) using Bowtie2 (Langmead and Salzberg 2012), with only PE reads with a total distance between reads of 120 and 180 bp to denote mono-nucleosomes used in subsequent analyses; nucleosome positions were determined and nucleosome peaks were smoothed with the program NucWave (Quintales *et al.* 2014). Nucleosome signals relative to genomic position were determined with the program SitewriterCFD.pl (Kent *et al.* 2010; Gal *et al.* 2015) using bed files of the transcriptional start sites (TSSs) all, up-, and downregulated genes, or genes that are near (<500 bp) or distant (~7500 bp) from cytosine methylation peaks; all region bed files were modified as four-column input site files for SitewriterCFD.pl (provided in File S2). For average enrichment profiles, average nucleosome signal was graphed in Excel, while for heatmaps, individual loci signal matrices were normalized to the average signal (in Excel), clustered (Cluster 3.0) (de Hoon *et al.* 2004) or reordered relative to other clusters (custom python script; File_S3-Arrange_clusters_Arguments), and plotted as heatmaps (Java TreeView) (Saldanha 2004). SitewriterCFD.pl was also used to calculate cytosine methylation signal relative to genomic position using single base pair resolution input files generated in UNIX by replacing cytosine methylation signal data into a single base zero-signal position file.

Data availability

All ChIP-sequencing, MNase-sequencing, bisulfite-sequencing, and RNA-sequencing data sets, as well as genome position files, have been deposited to the NCBI Gene Expression Omnibus (accession number GSE98911). Supplemental Figure files (Figures S1–S20 and File S1), data sets (File S2), and program (File S3) have been deposited to Figshare. Reagents, including strains, are available upon request. Supplemental material available at Figshare: https://doi.org/10.25386/genetics.7210190.

Results

Identification of the dim-1 gene

The Neurospora *dim-1* strain has a ~50% reduction in DNA methylation at constitutive heterochromatin (see Figure 1, A and B) (Foss *et al.* 1993), and was initially mapped to a large region of the right arm of Linkage Group III (Foss *et al.* 1998). To identify the defect responsible for this methylation defect, we sequenced the genomes of two *dim-1* strains (N654 and N1072) derived from one of the three independent isolates from the original selection (Foss *et al.* 1993). A nonsense mutation (S224stop) was identified in gene NCU06484 in the *dim-1* strains and we confirmed that this mutation was absent from the parental *mus-20* strain (N200). Sanger sequencing of NCU06484 from an independent *dim-1* mutant strain (N1634; Figure S1) revealed a nonsense mutation at Q1754, supporting the idea that NCU06484 is *dim-1*. The predicted protein encoded by NCU06484 is 1955 amino acids long and has orthologs that share significant sequence similarity in organisms from yeast to humans (File S1). The DIM-1 primary structure includes two AAA-ATPase domains,

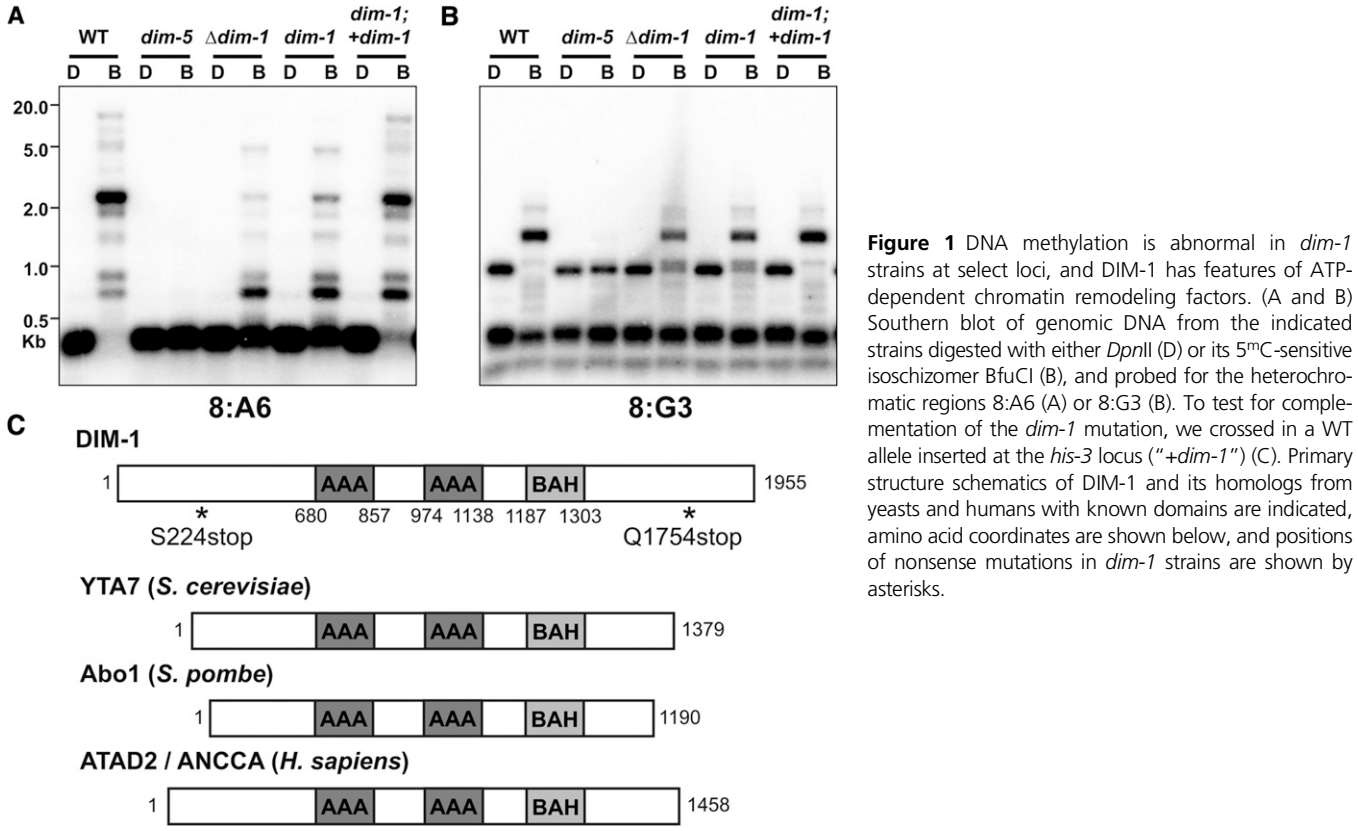

Figure 1 DNA methylation is abnormal in *dim-1* strains at select loci, and DIM-1 has features of ATP-dependent chromatin remodeling factors. (A and B) Southern blot of genomic DNA from the indicated strains digested with either *Dpn*II (D) or its 5^{m}C-sensitive isoschizomer BfuCI (B), and probed for the heterochromatic regions 8:A6 (A) or 8:G3 (B). To test for complementation of the *dim-1* mutation, we crossed in a WT allele inserted at the *his-3* locus ("*+dim-1*") (C). Primary structure schematics of DIM-1 and its homologs from yeasts and humans with known domains are indicated, amino acid coordinates are shown below, and positions of nonsense mutations in *dim-1* strains are shown by asterisks.

a weakly predicted BAH domain, and a positively charged N terminus (Figure 1C); the latter two structural elements suggest DIM-1 may interact with histones (Lombardi *et al.* 2011). This gene product was previously identified as "clock ATPase" (CATP) because of an apparent role in altered circadian rhythm (see *Discussion*) (Cha *et al.* 2013). Further, we analyzed DNA methylation in a strain harboring a complete deletion of NCU06484 (N5496) and found a loss of methylation at constitutive heterochromatin comparable to that of the strains harboring the *dim-1* nonsense mutations (Figure 1, A and B). Finally, we found that the hypomethylation phenotype of a *dim-1* strain was complemented by expression of an ectopic, FLAG-tagged *dim-1* gene (Figure 1, A and B and Figure S2), confirming that the mutations within NCU06484 are responsible for the Dim phenotype.

Hyper-methylation at intergenic regions in dim-1 strains

Early assessments of DNA methylation in *dim-1* strains by Southern hybridization suggested that the defect does not uniformly reduce DNA methylation (Foss *et al.* 1998). Unlike effects of reducing methylation with 5-azaC treatment or methionine starvation (Roberts and Selker 1995), differential changes were observed at the sites tested. To characterize the effect of *dim-1* on DNA methylation globally, we performed whole genome bisulfite-sequencing on WT and *dim-1* strains bearing either the S224stop allele (N1634) or a full deletion of the gene (Δ*dim-1*; N5496). Bisulfite-sequencing confirmed the substantial hypomethylation in *dim-1* strains detected by Southern hybridizations at regions of constitutive heterochromatic (Figure 2A and Figures S3, A and B and S4). Surprisingly, however, both *dim-1* strains also showed numerous new peaks of cytosine methylation, as illustrated for Linkage Group VI (Figure 2A and Figure S3, A and B; other chromosomes are shown in Figure S4). The hyper-methylation was found predominantly at intergenic regions but also in some gene bodies. Representative examples of this aberrant methylation were confirmed by Southern hybridizations (Figure 2, B and C and Figure S3C); control Southern blots, *e.g.*, with a fragment of the unmethylated *am* gene body (Figure S3D), verified that the digests were complete. Average enrichment profiles, which display the average sequencing signal across the examined regions, revealed that while overall methylation was reduced ~50% in constitutive heterochromatin (Figure 2D and Figure S3E top), when all methylated regions are considered (constitutive heterochromatin plus the "neo-heterochromatin" in *dim-1* strains), the hyper-methylation and hypomethylation largely cancel each other such that *dim-1* and WT strains show similar levels of cytosine methylation (5^{m}C) overall (Figure S3E, middle). Some spreading of 5^{m}C in *dim-1* beyond the normal heterochromatin boundaries was also observed, *e.g.*, at 8:G3 (Figure 2A and Figure S3A) and 8:A6 (Figure S3B) and as shown in the average enrichment profiles of aggregated data sets (Figure S3E, middle). Interestingly, close examination of only the regions that became hyper-methylated in *dim-1* strains revealed traces of DNA methylation in the WT strain

(Figure 2E and Figure S3, A, B, and E bottom). Methylation patterns of strains with deletion or nonsense alleles were very similar but effects of the deletion appeared more pronounced in some assays (Figures S3, A, B, and E and S4). We confirmed that the DNA methyltransferase DIM-2 is required for the aberrant cytosine methylation in Δ*dim-1* (Figure S5) and found that the hypomethylation of constitutive heterochromatin regions was not rescued by overexpression of *dim-2* when a second copy of the gene was inserted at an ectopic locus (Figure S6).

We considered the possibility that the novel methylation was directed by small interfering RNAs, such as Dicer-independent small interfering RNAs (disiRNAs) that have been implicated in low-level methylation associated with antisense or convergent transcription (Lee *et al.* 2010; Dang *et al.* 2016). To test this, we deleted the *eri-1*gene, which encodes the RNase necessary for disiRNA and disiRNA locus DNA methylation (Dang *et al.* 2016). Loss of ERI-1 did not abolish the peaks of cytosine methylation that appear in *dim-1* mutants (Figure S7), ruling out this possibility.

Altered enrichment of post-translational histone marks in dim-1 strains

Considering that cytosine methylation in *N. crassa* depends on H3K9me3, we compared the distribution of this mark in Δ*dim-1* and WT strains by ChIP-sequencing. The patterns of H3K9me3 in the strains were similar but the Δ*dim-1* strain showed additional peaks of H3K9me3 associated with the new peaks of intergenic DNA methylation (Figure 2A and Figures S3B and S4). The new H3K9me3 peaks in *dim-1* were often smaller (average of ~2000 bp) and less intense than those in constitutive heterochromatic regions of WT strains. This general difference was observed with two different peak-call pipelines, MACS2 and SICER (Zhang *et al.* 2008; Xu *et al.* 2014), although details varied, with SICER detecting fewer new peaks than MACS2 (File S2). The gain of H3K9me3 peaks did not appreciably increase global H3K9me3 levels (Figure S3F). An average enrichment profile analysis of H3K9me3 ChIP-sequencing from Δ*dim-1* strains showed nearly equivalent levels of H3K9me3 in constitutive heterochromatic regions as defined in a WT strain (Figure 2F and Figure S8A) plus minor spreading of H3K9me3 beyond the heterochromatic region borders. When the neo-heterochromatin of the Δ*dim-1* was also considered, however, the mutant showed increased H3K9me3 levels (Figure S8B). Considering just the intergenic regions associated with new DNA methylation revealed substantially increased H3K9me3 (Figure 2G and Figure S8C). As expected, all H3K9me3 associated with neo-heterochromatin was found to require DIM-5 (Figure S9). Unlike the highly AT-rich constitutive heterochromatin sequences that are normally methylated, the base composition was found to be only slightly enriched for A:T base pairs in the regions hyper-methylated in the Δ*dim-1* strain (Figure 2, H and I). Silencing associated with constitutive heterochromatic regions was not noticeably affected by *dim-1* (Figure S10).

We considered whether the mark of facultative heterochromatin, H3K27me2/3, might be also affected by deletion of *dim-1*. ChIP-sequencing of H3K27me2/3 showed some, but relatively few, differences in the level and/or distribution of this mark in WT and Δ*dim-1* strains (Figure S11); a peak analysis showed that 11 minor peaks were lost and 45 peaks were gained, (File S2), and some peaks present in both WT and Δ*dim-1* strains became more and less prominent in the Δ*dim-1* strain (Figure S11, top and bottom, respectively). In addition, one region of constitutive heterochromatin had a reduction in H3K9me3 but gained H3K27me2/3 (Figure S11, top).

Transcriptional effects of deletion of dim-1

Unlike *Neurospora* strains bearing a deletion of the DNA MTase gene, *dim-2*, which grow well (Honda *et al.* 2012), Δ*dim-1* strains grow slowly (Figure S12). This suggested that the DNA hyper-methylation observed in euchromatic regions of *dim-1* strains affects gene expression. We explored this possibility by carrying out RNA-sequencing on poly-A mRNA from Δ*dim-1* and WT strains. In the Δ*dim-1* strain, 601 genes were significantly upregulated, and 958 genes were significantly downregulated relative to the WT strain (File S2). Given that many of the newly methylated regions are at promoter regions, we wondered if establishment of heterochromatin at promoters repressed gene expression. Of the 958 downregulated genes, only 155 (16.2%) showed cytosine methylation of at least 200 bp within 500 bp of the predicted TSSs (File S2). Consistent with the weak correlation between new cytosine methylation and reduced gene expression, average enrichment profiles of $5^{m}C$ across up- and downregulated genes in Δ*dim-1* showed minor changes in methylation and these were not correlated with changes in gene expression (Figure S13, A and B). It remains possible that methylation changes indirectly affect gene expression. Interestingly, the highest expressed quartile of genes in WT showed the greatest new cytosine methylation in the Δ*dim-1* strain, which is mostly in promoter regions and somewhat in 3′UTR regions (Figure S13C). Silent genes showed little cytosine methylation associated with their 5′ and 3′ regions (Figure S13D).

Loss of DIM-1 alters nucleosome positions genome- wide

The substantial changes in gene expression detected in *dim-1* strains are consistent with the possibility that DIM-1 serves as an ATP-dependent chromatin remodeling factor ("chromatin remodeler"). DIM-1 includes two ATPase domains and two regions that may facilitate histone interactions, a weakly conserved BAH domain and a positively charged N terminus (Figure 1C), and is homologous to chromatin remodelers in other species, including Yta7 in *Saccharomyces cerevisiae*, Abo1 in *Schizosaccharomyces pombe*, and ANCCA/ATAD2 in humans (Figure 1C and File S1) (Zou *et al.* 2007; Revenko *et al.* 2010; Lombardi *et al.* 2011; Gal *et al.* 2015). Indeed, DIM-1 was reported as a CATP involved in the *Neurospora* circadian clock and has been

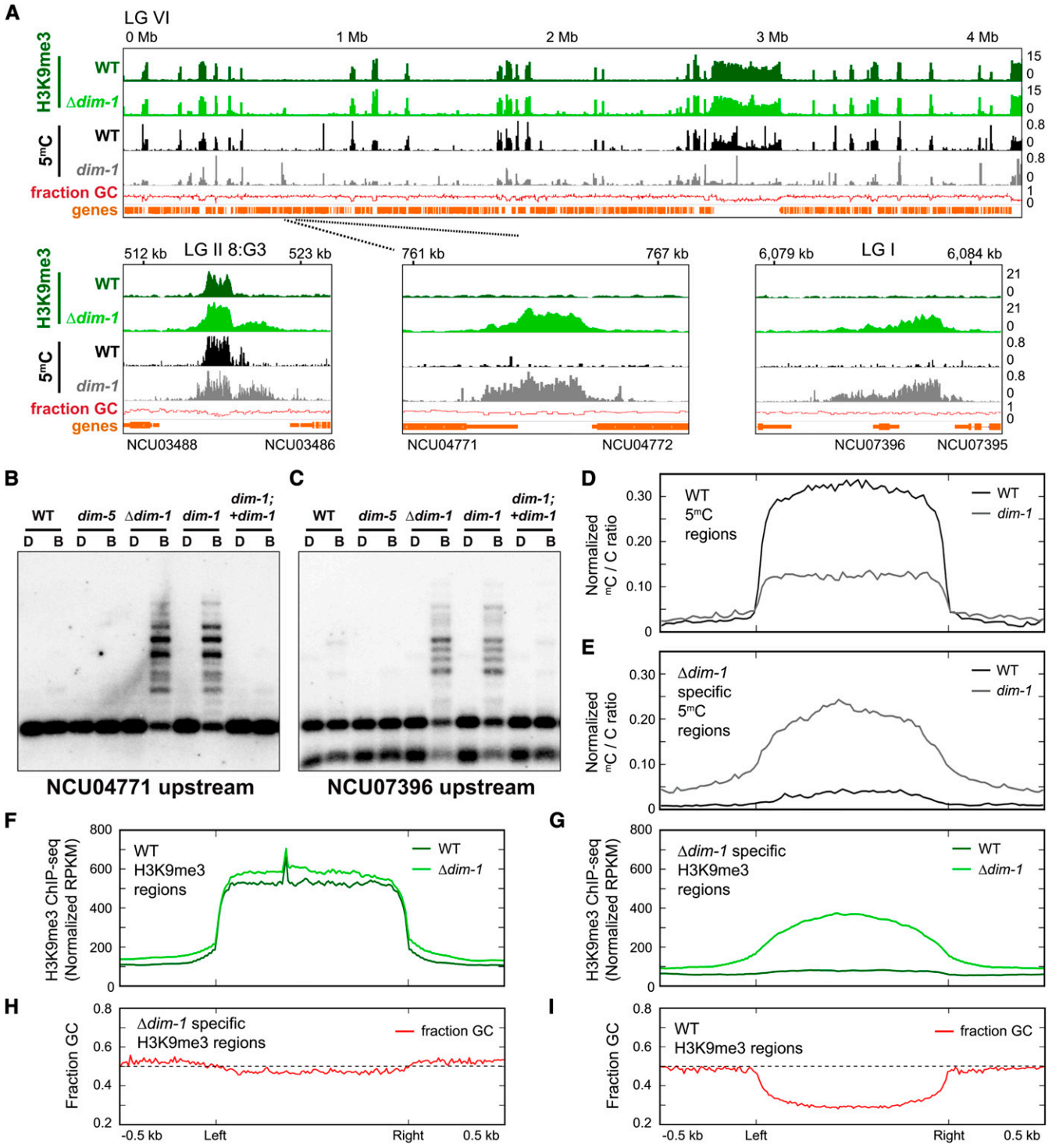

Figure 2 DNA methylation and H3K9me3 are abnormal in *dim-1* strains genome-wide. (A) ChIP-sequencing tracks (merged replicates) for H3K9me3 (green) or bisulfite-sequencing for cytosine methylation (black/gray) for WT or *dim-1* strains, and base composition ("fraction GC," red); all tracks are displayed in 25 bp windows. LG VI is shown, but comparable results were obtained for the other six chromosomes (Figure S4). Selected regions are shown expanded below; different chromosomes [Linkage Groups (LGs)] are identified. Tracks here and in other figures are displayed with the Integrative Genomics Viewer (Robinson *et al.* 2011) with coordinates relative to the left telomere, and NCU numbers of genes, shown above and below, respectively. (B and C) Southern blots of genomic DNA from the indicated strains digested with either *Dpn*II (D) or its 5^{m}C-sensitive isoschizomer BfuCI (B) and probed for the labeled regions, as in Figure 1A; "upstream" denotes the intergenic region upstream of that gene. (D and E) Average enrichment profiles of bisulfite-sequencing data showing the ratio of methylated-to-unmethylated cytosines across H3K9me3-marked regions in WT strains (D; n = 210) or specifically found in Δ*dim-1* strains (E; n = 239). Plots show 500 bp upstream and downstream of the left and right borders of constitutive heterochromatic regions, which were scaled to 1 kb for presentation. y-axis denotes the normalized ratio of methylated cytosines/total cytosines per

shown to affect nucleosome occupancy at the C-box enhancer element of the *frequency* locus (Cha *et al.* 2013). To further investigate the possibility that DIM-1 is a chromatin remodeler, we tested MNase sensitivity of chromatin from WT and Δ*dim-1* strains. We first performed MNase time-course experiments, gel-fractionated the products, and probed for various genomic regions. The terminal time points showed predominantly mono- and di-nucleosome populations (Figure 3A, EtBr). Curiously, in both strains, heterochromatic regions (2:B3 and 8:A6) appeared to be digested to mono- and di-populations somewhat faster than the euchromatic region (*his-3*), perhaps due to differences of base composition or accessibility. In addition, heterochromatic nucleosomes appeared more disordered than their euchromatic counterparts. Nucleosome bands for both the euchromatic (*his-3*) and heterochromatic (2:B3 and 8:A6) regions appeared "fuzzier" in chromatin from the Δ*dim-1* strain than those from WT, suggestive of greater nucleosome disorder in the mutant (Figure 3A). Results for an intergenic region that has aberrant hyper-methylation in *dim-1* (NCU04771 upstream) were also suggestive of nucleosome alterations in a *dim-1* strain, with multiple poorly defined nucleosomes rather than predominately a single nucleosome at this region of WT (Figure 3A, right). The Southern probe covers the nucleosome-free region (NFR) of NCU04771, raising the possibility that this NFR in a Δ*dim-1* strain has increased, albeit variable, nucleosome occupancy, as has been reported for Yta7 in *S. cerevisiae* (Lombardi *et al.* 2011).

To characterize nucleosome positioning genome-wide, we performed paired-end sequencing of mono-nucleosomes isolated from moderately digested chromatin of Δ*dim-1* and WT strains (time points indicated by arrow heads in Figure 3A). Results from replicates covered the entire genome and were highly reproducible (Figure S14), giving us confidence in the significance of observed differences and allowing us to merge the data for subsequent analyses. Alignment of all genes with the presumptive TSSs (n = 8668) revealed that nucleosome peaks in the Δ*dim-1* strain were progressively shifted slightly toward the 5′ ends of genes; the nucleosome length was shortened by roughly 6 bp (Figure 3B), which became obvious by the third (+3) nucleosome (Figure 3B). An equivalent effect had been reported for the budding yeast homolog of DIM-1 homolog, Yta7 (Lombardi *et al.* 2014). Given that Yta7 has been reported to be a regulator of histone H3 (hH3) expression (Gradolatto *et al.* 2008; Fillingham *et al.* 2009), we checked whether expression of hH3 (NCU01635) in the Δ*dim-1* strain was similar to that of a WT strain and found that it was (File S2, RNA-sequencing). We also found that addition of an ectopic *hH3* gene did not rescue the Δ*dim-1* phenotype (Figure S15), suggesting that changes in *hH3* levels were not responsible for the differences in nucleosome positioning.

Considering that a global analysis of nucleosome positioning of all genes might hide some DIM-1-specific nucleosome changes, we examined nucleosome positioning at the TSS of subsets of genes, including those whose expression or DNA methylation changed in Δ*dim-1*. Genes with decreased expression showed the most substantial changes in nucleosome positions in average enrichment profiles (Figure S16A). Genes whose expression increased, or did not change, in a Δ*dim-1* strain seemed to exhibit less change (Figure S16, B and C). Examination of individual genes supported the suggestion that the *dim-1* defect leads to differences in nucleosome positioning, as illustrated for downregulated NCU08052 (Figure 3C, top). Genes that did not have substantial changes in expression and those that were upregulated appeared to maintain nucleosome positioning better, as illustrated by NCU04402 (Figure 3C, bottom) and NCU03598 (Figure S16D). We also tested if changes in nucleosome positioning correlated with changes in DNA methylation at nearby genes. An average enrichment profile of 541 genes whose TSS was within 500 bp of a new peak of cytosine methylation in a Δ*dim-1* strain showed modest changes in nucleosome arrangement (Figure S16E) but similar changes were observed with control regions farther (∼7500 bp) from the new cytosine methylation (Figure S16F).

We next investigated nucleosome positions in constitutive heterochromatin of WT and *dim-1* strains. Our survey, performed on 210 regions of H3K9me3 in WT, resulted in two conclusions: (1) Relative to euchromatin, nucleosomes in the regions of constitutive heterochromatin appear irregular/disordered; and (2) this disorder is exacerbated by loss of DIM-1. Examination of representative regions of the constitutive heterochromatin reveal that the nucleosome peaks were shorter and broader than in the adjacent chromatin (*e.g.*, see Figure 4A), both in the WT and Δ*dim-1* strains, presumably reflecting irregularly spaced nucleosomes. Differences between the strains were also evident though somewhat subtle. Especially in the WT strain, the heterochromatin was typically flanked by strong border nucleosomes. Although more disordered, internal nucleosomes sometimes showed some regularity, especially in the WT strain (see Figure 4A, left, black arrow). The relative disorder of nucleosomes in the heterochromatin of the Δ*dim-1* may partly relate to fact that H3K9me3 exhibits spreading in the mutant beyond the normal heterochromatin boundary (*e.g.*, see Figure 4A, right, red arrow). To further explore the difference in nucleosome arrangement between heterochromatin and euchromatin in Δ*dim-1* and WT strains, we generated average enrichment profiles and heatmaps to display the nucleosome signals

amount of sequencing genome coverage. (F and G) Average enrichment profiles, as in D and E, but of H3K9me3 ChIP-sequencing enrichment in WT and Δ*dim-1* strains merged from two experiments; *y*-axis denotes the normalized amount of ChIP-sequencing reads per kilobase per million total reads (RPKM). (H and I) Average enrichment profiles, as in B and C, but of fraction of GC base pairs; horizontal line marks the position where base composition is 50% G+C.

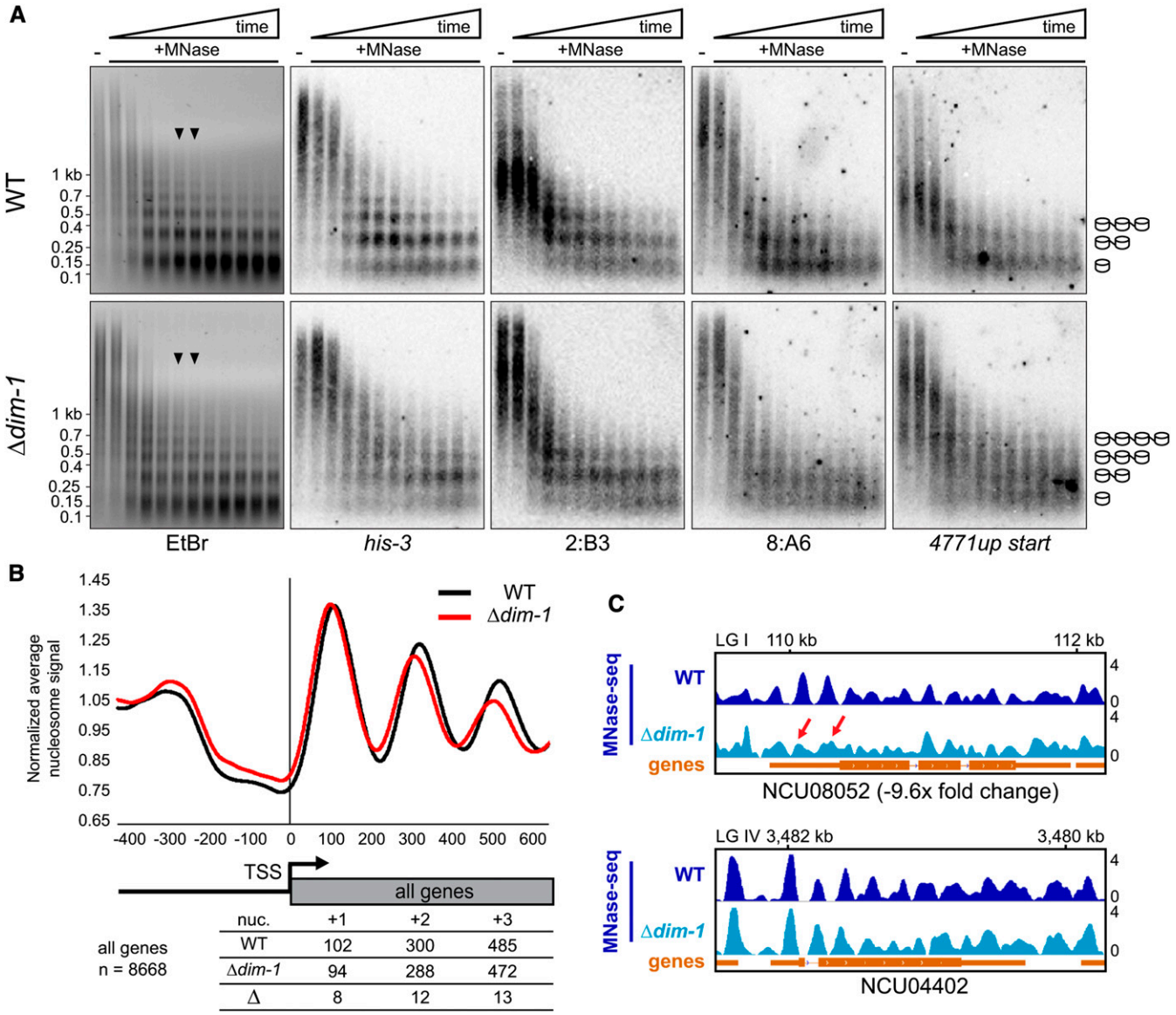

Figure 3 Nucleosome positioning is altered at the TSSs of genes in Δ*dim-1* strain. (A) Southern blots of DNA from 20-min time course micrococcal nuclease (MNase) digest with WT and Δ*dim-1* nuclei, probed for the indicated regions; the "NCU04771up start" probe covers the intergenic promoter region of gene NCU04771, including the nucleosome-free region. Arrowheads indicate the time points (8 and 10 min) from which mono- and di-nucleosomes and intervening DNA was purified for paired-end high-throughput sequencing (below). Cartoons at right show interpretation of nucleosome patterns leading to smallest fragments. (B) Average nucleosome enrichment profiles of MNase-sequencing data from WT and Δ*dim-1* strains normalized to the average signal across the 5′ end of all *Neurospora* genes, spanning 400 bp upstream to 600 bp downstream of the TSS; numbers below indicate the peak apices, in base pairs from the transcriptional start site (TSS) in WT and Δ*dim-1* strains, and the difference in the apex position, for the +1, +2, and +3 nucleosomes. (C) Representative examples of nucleosome positions in individual genes with changed (NCU08052), or unchanged (NCU04402; *dim-5*) expression in a Δ*dim-1* background. Red arrows highlight nucleosome disorder in a Δ*dim-1* strain of two nucleosomes that are well-positioned in a WT strain.

±500 bp of H3K9me3 regions. Alignments were to the first nucleosome within the H3K9me3 of the Δ*dim-1* (Figure 4, B and C) or WT (Figure 4, D and E) strains. The relative disorder of nucleosomes greatly limited the periodicity, especially in the Δ*dim-1* strain. Although even the WT strain showed limited nucleosome order (Figure 4B), the disorder of the *dim-1* strain was strikingly greater at both borders, independent of the reference nucleosome (Figure 4, B–E). A control analysis based on random genomic positions did not show patterning (Figure S17). Together, these analyses suggest that heterochromatic regions in WT *Neurospora* have inherent nucleosome disorder, and that nucleosomes in a Δ*dim-1* strain are even more disordered.

Interestingly, when we aligned bisulfite-sequencing data to the WT constitutive heterochromatin border, cytosine methylation showed an oppositely phased pattern relative to the nucleosome peaks in WT; *i.e.*, it occurs principally in linker DNA, consistent with the possibility that the DNA

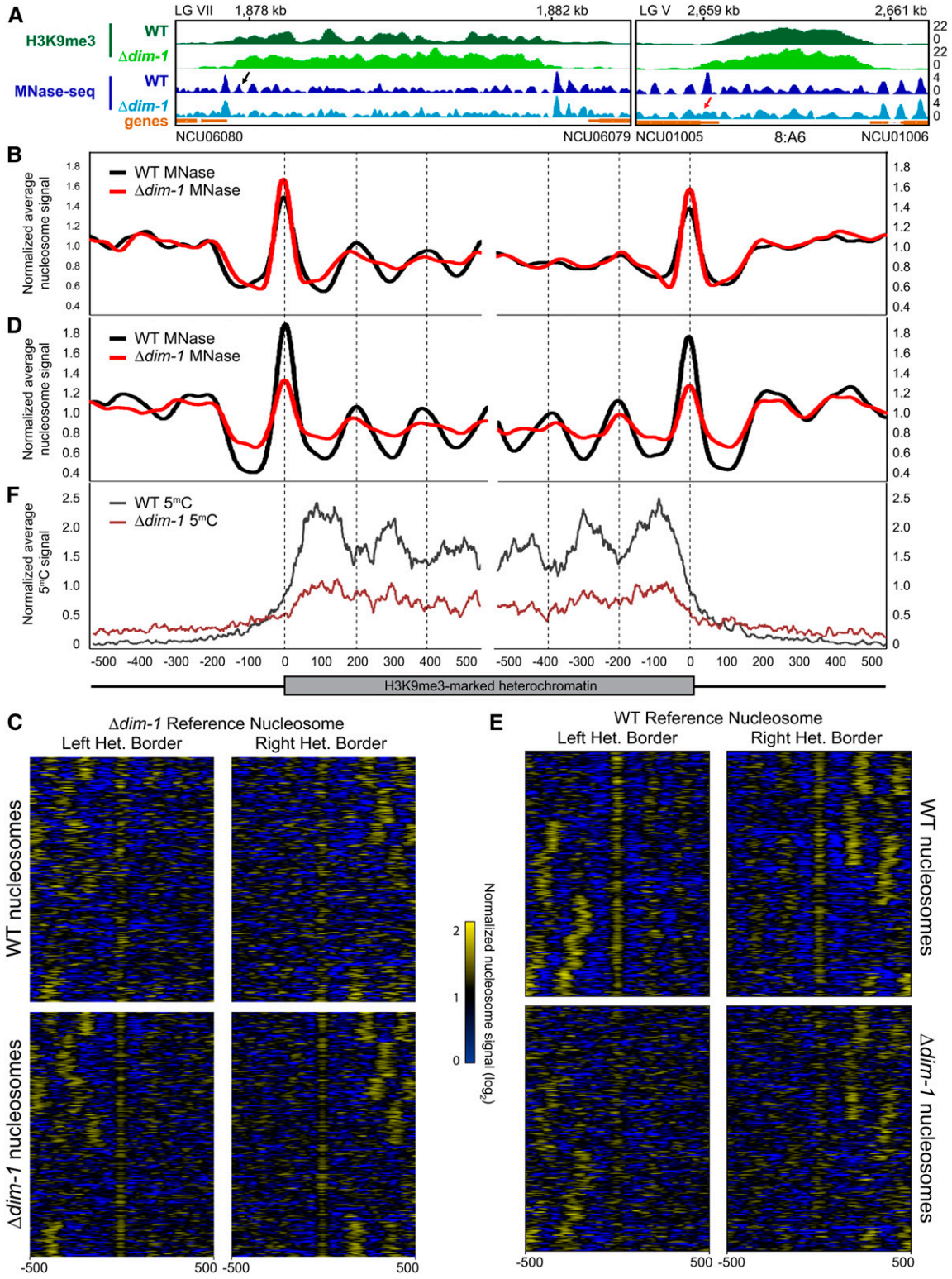

Figure 4 Constitutive heterochromatic regions exhibit nucleosome disorder, especially in Δ*dim-1* strains. (A) Representative examples of nucleosome positioning within constitutive heterochromatin. H3K9me3 ChIP-sequencing (green) and MNase-sequencing (blue) tracks of WT and Δ*dim-1* strains are shown for a region on LG VII between NCU06080 and NCU06079 and the 8:A6 region on LG V (Selker *et al.* 2003). The black arrow denotes an internal nucleosome that has periodicity in the WT strain while the red arrow denotes a border nucleosome that becomes disordered in the ?*dim-1* strain. (B) Average mono-nucleosome enrichment profiles of MNase-sequencing data (MNase) in WT and Δ*dim-1* strains at the left and right borders (relative to the left telomere) of constitutive heterochromatic regions longer than at least 1000 base pairs aligned from the first nucleosome peak completely covered by H3K9me3 in Δ*dim-1* strains. (C) Nucleosome peak signal heatmaps from WT and Δ*dim-1* strains normalized to the average enrichment signal. Data are shown for ±500 bp for the left and right heterochromatic region borders (n = 210) relative to the first heterochromatic nucleosome

methyltransferase DIM-2 has greater access to cytosines in linker DNA (Figure 4F, dark gray line). This pattern is not obvious in DNA of the Δ*dim-1* strain and cytosine methylation is consistently lower across the constitutive heterochromatin region (Figure 4F, maroon line).

Although we did not observe marked changes in nucleosome positions around the TSSs of genes near neo-heterochromatin, we did find significant changes in the position of nucleosomes in intergenic regions that gain cytosine methylation in *dim-1* strains. This was evident both by inspection of individual regions (Figure 5A) and in average enrichment profiles and heatmaps (Figure 5, B and C). Nucleosome peaks in the Δ*dim-1* strain were more numerous, lower, and broader than in the WT strain (Figure 5A). This is consistent with the increased nucleosome laddering from reduced MNase accessibility observed by Southern hybridizations (Figure 3A) and suggests that nucleosome positions are destabilized by loss of DIM-1. Average enrichment profiles of nucleosome and bisulfite-sequencing signals at the borders of these regions and at a randomly chosen, more central nucleosome showed reduced signals indicating reduced nucleosome positioning, especially of those nucleosomes internal to the neo-heterochromatin borders (Figure 5B), a conclusion reinforced by the heatmaps showing the position of nucleosomes at each region analyzed (Figure 5C). The cytosine methylation that appeared in the Δ*dim-1* strain showed no clear periodicity comparable to that normally found in heterochromatin. Together, these data reinforce the notion that regions gaining cytosine methylation in a Δ*dim-1* strain have relatively disordered nucleosomes.

We decided to take advantage of the fact that DIM-1 is highly expressed in WT cells (Figure S18A), to seek information on interacting proteins by mass spectroscopy of coimmunopurified proteins. DIM-1-3xFLAG pulled-down histones H1, H2A, H2B, H3, H4, the H2A.Z histone variant, and two uncharacterized proteins encoded by NCU00856 and NCU03126 (Figure S18B). Mass spectroscopy of proteins associated with NCU00856-3xFLAG revealed only interactions with DIM-1 and histones (Figure S19A) and deletion of NCU00856 did not cause a phenotype comparable to that of *dim-1* mutants, *i.e.*, aberrant methylation (Figure S19B). The association with histones and the above defects in nucleosome positioning are consistent with the possibility that DIM-1 is chromatin remodeler.

DIM-1 localizes to regions gaining aberrant cytosine methylation

To explore the possibility that the regions of hyper-methylation in *dim-1* strains are direct targets of DIM-1 action, we examined DIM-1 localization. Attempts to map DIM-1 by ChIP were unsuccessful, leading us to turn to DamID (Vogel *et al.* 2007; Lewis *et al.* 2010b), in which the DNA adenine MTase gene from *Escherichia coli* was fused to DIM-1 so that its location could be inferred by the pattern of adenine methylation at GATC sites. Genomic DNA was digested with *Dpn*II, which is inhibited by adenine methylation in GATC sites, or by the isoschizomer *Dpn*I, which specifically cleaves when the adenine is methylated. Although little adenine methylation was observed at a centromere or at a euchromatic region not subject to new cytosine methylation (NCU01597), substantial adenine methylation was detected at an interspersed heterochromatic region (8:G3; Figure 6A and Figure S20A) and at euchromatic regions gaining aberrant hyper-methylation in Δ*dim-1*, such as the NCU04771 and NCU07396 upstream regions and the *am* locus (Figure 6A and Figure S20, B and C). Control DamID constructs for the DNA MTase DIM-2 and the H3K9 MTase DIM-5 gave adenine methylation at centromeres but not NCU01597 (Figure 6A and Figure S20A). Surprisingly, DIM-2-DAM and DIM-5-DAM also localized to the regions that are subject to hyper-methylation, even in *dim*$^+$ strains (Figure 6A and Figure S20C).

To investigate which domains of DIM-1 are required for its function and localization, we individually deleted the positively charged N terminus or the BAH domain of DIM-1. These deletion constructs had reduced expression compared to the WT DIM-1 protein when protein levels were assayed through 3xFLAG immunoblotting. Neither mutant complemented the *Δdim-1* hyper-methylation phenotype, suggesting these domains are important for DIM-1 function or the expression levels were not sufficient (Figure S20D). We used DAM fusion proteins to test localization. The ΔBAH domain DIM-1-DAM construct still exhibited significant localization to promoter regions that are hyper-methylated, indicating the BAH domain is not critical for localization (Figure S20D, middle). The ΔN terminus DIM-1-DAM construct showed no *Dpn*I-specific cleavage, possibly due to low levels of expression.

To explore the relationship between DIM-1 localization and hyper-methylation, we examined DIM-1-DAM localization, as inferred from adenine methylation, in the presence or absence of DIM-2, and similarly examined localization of DIM-2 in the presence or absence of DIM-1. Loss of DIM-1 caused a modest increase in localization of DIM-2-DAM to an upstream region that becomes hyper-methylated, as evidenced by the increased cleavage of *Dpn*I (Figure 6B, left). Conversely, loss of DIM-2 increased DIM-1-DAM targeting, as shown by the near-complete *Dpn*I cleavage (Figure 6B, left). No comparable changes were observed at a constitutive heterochromatic region (Figure 6B, right).

Discussion

We determined that *Neurospora dim-1* encodes a putative AAA ATPase chromatin remodeler and results in both hypo- and hyper-methylation; Figure 6C summarizes the phenotypes

peak in Δ*dim-1* strains. Heterochromatic regions are identically ordered in each heatmap group. (D) Average mono-nucleosome enrichment profiles of MNase-sequencing data (MNase) in WT and Δ*dim-1* strains at the left and right borders, as in B. Vertical dashed lines mark the apices of WT nucleosome signals. (E) Nucleosome peak signal heatmaps from WT and Δ*dim-1* strains normalized to the average enrichment signal, as in C, relative to the first heterochromatic nucleosome peak in WT strains. (F) Average enrichment profiles of bisulfite-sequencing showing enrichment of cytosine methylation in WT and Δ*dim-1* strains at the left and right borders of constitutive heterochromatic regions.

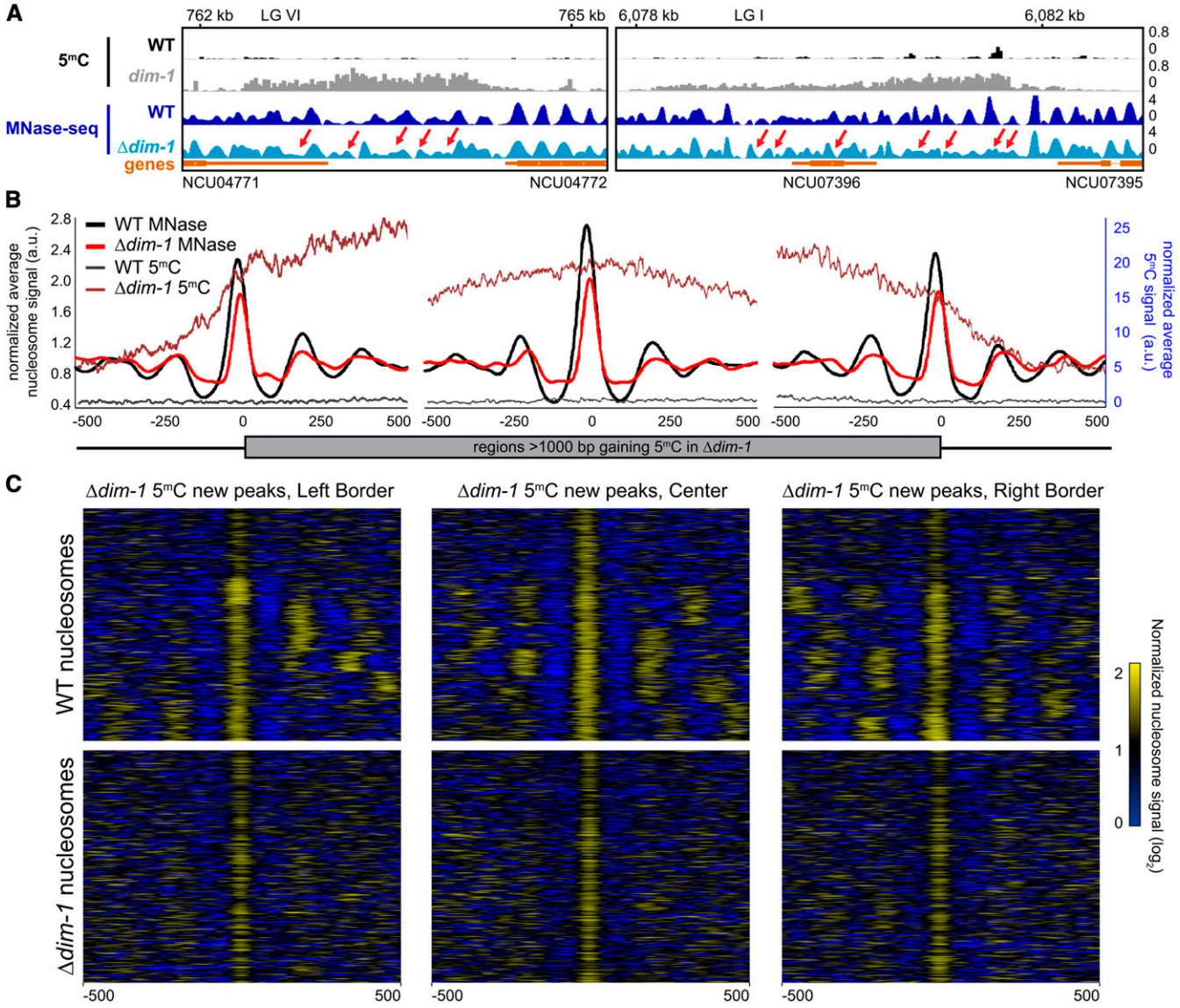

Figure 5 Intergenic regions that gain cytosine methylation in Δ*dim-1* exhibit aberrant nucleosome positioning. (A) Representative examples of nucleosome positions within intergenic regions that gain cytosine methylation. Tracks of bisulfite-sequencing for WT (black) and *dim-1* (light gray), as well as MNase-sequencing for WT (dark blue) and Δ*dim-1* (light blue) strains are shown. Red arrows highlight changes in nucleosome positioning in Δ*dim-1* strain. (B) Average mono-nucleosome enrichment profiles (MNase) and cytosine methylation (5^mC) in WT and Δ*dim-1* strains at the first nucleosome apex in left and right borders of regions that gain methylation in a *dim-1* strain, as well as a central reference nucleosome peak in a WT strain ($n = 322$); the WT data used reference nucleosomes in a WT strain while the *dim-1* data used reference nucleosomes from a Δ*dim-1* strain. (C) Heatmaps of nucleosome signals from WT and Δ*dim-1* strains normalized to average nucleosome signal examining ±500 bp of the intergenic regions gaining cytosine methylation in Δ*dim-1* strain shown in B; regions are shown in each heatmap pair in the same order.

of a *dim-1* strain. The original *dim-1* mutants were obtained in a selection scheme based on the observation that DNA repair–defective strains (*e.g.*, a *mus-20* mutant) were hyper-sensitive to 5-azaC, potentially due to defective repair of adducts between 5-azaC in DNA and a DNA MTase. However, no MTase mutants were identified and deletion of the gene encoding the only cytosine MTase in the genome, *dim-2*, did not alleviate the 5-azaC sensitivity of *mus-20* strains (Foss *et al.* 1998). We found that DIM-1 is not only required for WT levels of DNA methylation at constitutive heterochromatin, the first observed phenotype (Foss *et al.* 1998), but also prevents aberrant hyper-methylation in intergenic regions. These regions of hyper-methylation showed aberrantly positioned nucleosomes as well as greater, but variable, nucleosome density, indicating that DIM-1 is essential for proper nucleosome positioning and occupancy, similar to Yta7 in *S. cerevisiae* (Lombardi *et al.* 2011, 2014). While speculative, one possibility for the intergenic methylation is that nucleosome disorder creates a nucleosomal pattern that resembles constitutive heterochromatin, where the underlying AT-rich

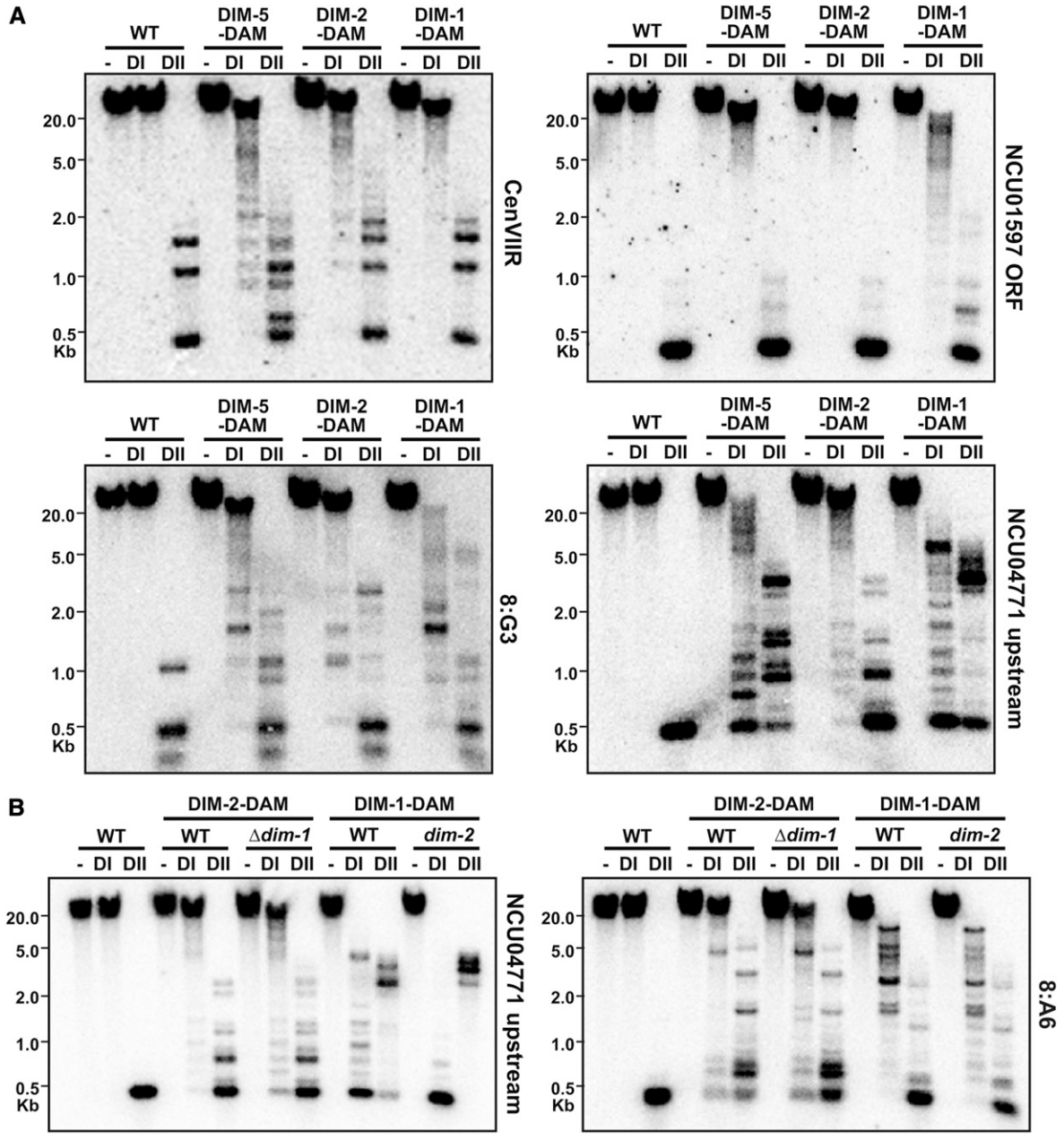

C

Constitutive Heterochromatin type	AT-rich	DIM-2/5 target	DIM-1 target	5mC		Nucleosomes		5mC Periodicity	
				WT	*dim-1*	WT	*dim-1*	WT	*dim-1*
Interstitial (*e.g.*, 8:A6, 8:G3)	Moderate	+	+	High	Moderate	Strong border; less ordered than euchr.	Disordered	+	-
Centromeric	High	+	-	Moderate	Low	Disordered	Disordered	N.D.	N.D.
"Neo" (*dim-1*-specific)	Slight	+	+	Trace	Moderate	Ordered	Disordered	N/A	-

Figure 6 *DIM-1* and heterochromatin machinery localize to heterochromatic regions and intergenic regions. (A) DamID Southern blots of genomic DNA of the indicated *dim*$^+$ strains digested with *Dpn*I (cuts GA^{m}TC; DI) or its isoschizomer *Dpn*II (inhibited by adenine methylation; DII) or left undigested (−) and probed for the indicated regions. (B) DamID Southern blots, as in A, for different mutant backgrounds expressing the indicated DAM fusion constructs. (C) Table summarizing the phenotypes of a *dim-1* strain. N.D., not determined.

DNA may allow for nucleosome "slippage" or otherwise signals the heterochromatic machinery. The gain in intergenic methylation was, at best, weakly correlated with high levels of overall gene expression, despite hundreds of genes being downregulated in Δ*dim-1* strains. This discrepancy may reflect the sensitivity of these promoters to changes in the arrangement of nucleosomes around the TSS and not increased levels of cytosine or histone methylation.

Curiously, even in a WT background, the H3K9 MTase, DIM-5, the DNA MTase, DIM-2, and DIM-1 all strongly localize to the intergenic regions that become aberrantly methylated in *dim-1* strains. This gives the impression that the heterochromatin machinery is "poised" at these regions and DIM-1 may regulate nucleosome occupancy at these loci by responding to H3K9me3 and $5^{m}C$ levels. Interestingly, deletion of *dim-2* allows DIM-1 to localize to a greater extent at these intergenic regions. Regions of constitutive heterochromatin in Δ*dim-1* strains contain near WT levels of H3K9me3 that may remain high due to the presence of ample histone tails for DIM-5 action. These same regions contain roughly half the level of cytosine methylation observed in a WT strain. We noticed that the distribution of DNA methylation in WT *Neurospora* is higher in linker regions than in the nucleosomal DNA at constitutive heterochromatic regions, as reported for other species (Takeshima *et al.* 2008; Felle *et al.* 2011; Huff and Zilberman 2014), raising the possibility that the reduced periodicity and tighter packing of nucleosomes in a Δ*dim-1* strain reduces DNA methylation at constitutive heterochromatin by limiting accessible linker DNA. Consistent with this, elimination of the linker histone H1 slightly increases DNA methylation in *Neurospora* constitutive heterochromatin (Seymour *et al.* 2016). Cytosine methylation and H3K9me3 do not appear to be due to limiting DIM-2 or DIM-5, considering that additional copies of *dim-2* and *dim-5* did not rescue the methylation defects. Of course, we cannot exclude the possibility that unidentified factor(s) working in conjunction with DIM-1 affect DNA methylation, negatively or positively.

Interestingly, we found indications that heterochromatin is more sensitive than euchromatin to MNase digestion in *Neurospora*, which contrasts observations in *Drosophila* (Sun *et al.* 2001); of possible relevance, *Drosophila* does not contain a homolog of *dim-1* (Zou *et al.* 2007). The peaks of nucleosomes in *Neurospora* constitutive heterochromatin tend to be lower and broader than in euchromatin, implying irregular positioning (Lai and Pugh 2017). Because of repeat-induced point mutation (RIP), *Neurospora* constitutive heterochromatin is characterized by relatively simple, AT-rich DNA, which may contribute to movement of nucleosomes, resulting in the observed disorder (Lai and Pugh 2017); the known preference of MNase for A:T-rich DNA, or conceivably a preference for methylated DNA, could also contribute to the observed pattern of nucleosomes. It is intriguing that heterochromatin borders often have well-positioned nucleosomes, which may play a role in localizing protein complexes, such as the *Neurospora* DMM complex, that limit heterochromatin spreading (Honda *et al.* 2010).

The *dim-1* gene was independently identified as *catp* (clock ATPase) because a mutation of this gene resulted in aberrant circadian periodicity (Cha *et al.* 2013). The authors suggested that increased nucleosome occupancy could affect clock gene expression and reported increased histone H3 occupancy at the critical C-box enhancer element at the *frequency* gene (Cha *et al.* 2013). We showed that nucleosome positions are altered in gene bodies, heterochromatic regions, and intergenic regions genome-wide in a Δ*dim-1* strain, in accordance with observations in other organisms defective in homologs of DIM-1. In *S. pombe*, deletion of the comparable gene *abo1* leads to nucleosome disorder, and lower nucleosome signals are observed at gene bodies and transposable elements underlying heterochromatin (Gal *et al.* 2015). Moreover, in *S. cerevisiae*, loss of the DIM-1 homolog Yta7 causes a progressive shift of nucleosomes toward the 5′ end of genes (Lombardi *et al.* 2014). In a *Neurospora* Δ*dim-1* strain, nucleosome positions also shift toward the 5′ end of gene bodies, although the incomplete mapping of *Neurospora* TSSs undoubtedly contributes some "noise" to our analyses. While DIM-1, like Yta7, appears to maintain NFRs, the mechanism is unknown. NFRs in multiple species seem to depend on short, often directional AT tracts (Iyer and Struhl 1995; Segal and Widom 2009; Krietenstein *et al.* 2016; Lai and Pugh 2017) but we did not identify any strong NFR motifs in our analyses. Presumably, proper NFR positioning plays a role in the function of transcriptional machinery, accounting for observed changes in *dim-1* strains. In *S. pombe*, ABO1, interacts with the RNA Polymerase II–associated FACT complex to direct nucleosome assembly (Gal *et al.* 2015). Future studies may reveal specifics of changes in factor binding and gene expression resulting from changes in nucleosomal positioning.

DIM-1 is conserved among eukaryotes, and it is noteworthy that the human homolog ATAD2 (also known as ANCCA) (Zou *et al.* 2007, 2009; Boussouar *et al.* 2013) has a high level of sequence identity with DIM-1, Yta7, and ABO1, suggesting that ATAD2 is also an AAA ATPase chromatin remodeler. ATAD2 is a marker for multiple cancerous cell types: changes in expression of this protein is correlated with poor prognosis in multiple cancers (Zou *et al.* 2007, 2009; Ciró *et al.* 2009; Caron *et al.* 2010; Kalashnikova *et al.* 2010; Liu *et al.* 2012). Altered levels of ATAD2 cause misregulation of some oncogenes and influence epigenetic marks, such as increased levels of histone acetylation (Zou *et al.* 2007) and H3K4me3 (Revenko *et al.* 2010). In addition, ATAD2 overexpression is correlated with higher levels of the PRC2 member EZH2 in tumors (Kalashnikova *et al.* 2010), suggesting H3K27me levels could be affected. The ATAD2 bromodomain interacts with acetylated N-terminal tails of histone H3 and H4 (Ciró *et al.* 2009; Caron *et al.* 2010; Revenko *et al.* 2010). Although it is known that gene activation is diminished upon knockdown of ATAD2 (Zou *et al.* 2007, 2009; Revenko *et al.* 2010), and as such, ATAD2 acts as a transcriptional coactivator (Boussouar *et al.* 2013), little is known about the *in vivo* function of the protein. To the best of our knowledge, the level of

cytosine methylation/H3K9me3 or the position of nucleosomes have not been examined in ATAD2 deficient cancer cells. While downstream epigenetic changes may be different between oncogenic human cells and *Neurospora dim-1* strains, our discovery of aberrant cytosine methylation associated with altered nucleosome positioning in *Neurospora* Δ*dim-1* strains suggests that further studies in humans are warranted to learn if aberrant methylation, which is common in cancer, occurs in human cells with altered ATAD2 activity.

Acknowledgments

The authors would like to thank Josh Lowry and Will Storck (University of Oregon) for SNP identification and filtering help, Jeff McKnight (University of Oregon) for his help generating the MNase heatmap and for the use of his custom python script (File S3) for reordering nucleosome signal arrays, Neena Leggett for the initial bioinformatic analysis, all members of the Selker laboratory for helpful comments and discussions, Mark Johnston for title suggestions, and the three anonymous reviewers whose comments/suggestions helped improve the manuscript. Funding for this work was provided by grants from the National Institutes of Health (NIH) to E.U.S. (GM035690 and GM093061) and the Naito Foundation, the Nakajima Foundation, and the Ministry of Education, Culture, Sports, Science and Technology (MEXT)/Japan Society for the Promotion of Science (JSPS) Grants-in-Aid for Scientific Research (KAKENHI) (24870012), Japan, to S.H. A.D.K. was partly supported by an NIH postdoctoral fellowship (GM097821), and E.T.W. was partly supported by a fellowship from the American Heart Association (14POST20450071).

Literature Cited

Adhvaryu, K. K., E. Berge, H. Tamaru, M. Freitag, and E. U. Selker, 2011 Substitutions in the amino-terminal tail of Neurospora histone H3 have varied effects on DNA methylation. PLoS Genet. 7: e1002423. https://doi.org/10.1371/journal.pgen.1002423

Afgan, E., D. Baker, B. Batut, M. van den Beek, D. Bouvier *et al.*, 2018 The Galaxy platform for accessible, reproducible and collaborative biomedical analyses: 2018 update. Nucleic Acids Res. 46: W537–W544. https://doi.org/10.1093/nar/gky379

Allshire, R. C., and H. D. Madhani, 2017 Ten principles of heterochromatin formation and function. Nat. Rev. Mol. Cell Biol. 19: 229–244. https://doi.org/10.1038/nrm.2017.119

Boussouar, F., M. Jamshidikia, Y. Morozumi, S. Rousseaux, and S. Khochbin, 2013 Malignant genome reprogramming by ATAD2. Biochim. Biophys. Acta 1829: 1010–1014. https://doi.org/10.1016/j.bbagrm.2013.06.003

Bühler, M., and S. M. Gasser, 2009 Silent chromatin at the middle and ends: lessons from yeasts. EMBO J. 28: 2149–2161. https://doi.org/10.1038/emboj.2009.185

Caron, C., C. Lestrat, S. Marsal, E. Escoffier, S. Curtet *et al.*, 2010 Functional characterization of ATAD2 as a new cancer/testis factor and a predictor of poor prognosis in breast and lung cancers. Oncogene 29: 5171–5181. https://doi.org/10.1038/onc.2010.259

Cha, J., M. Zhou, and Y. Liu, 2013 CATP is a critical component of the Neurospora circadian clock by regulating the nucleosome occupancy rhythm at the frequency locus. EMBO Rep. 14: 923–930. https://doi.org/10.1038/embor.2013.131

Cingolani, P., A. Platts, L. Wang le, M. Coon, T. Nguyen *et al.*, 2012 A program for annotating and predicting the effects of single nucleotide polymorphisms, SnpEff: SNPs in the genome of *Drosophila melanogaster* strain w1118; iso-2; iso-3. Fly (Austin) 6: 80–92. https://doi.org/10.4161/fly.19695

Ciró, M., E. Prosperini, M. Quarto, U. Grazini, J. Walfridsson *et al.*, 2009 ATAD2 is a novel cofactor for MYC, overexpressed and amplified in aggressive tumors. Cancer Res. 69: 8491–8498. https://doi.org/10.1158/0008-5472.CAN-09-2131

Clapier, C. R., and B. R. Cairns, 2009 The biology of chromatin remodeling complexes. Annu. Rev. Biochem. 78: 273–304. https://doi.org/10.1146/annurev.biochem.77.062706.153223

Clapier, C. R., J. Iwasa, B. R. Cairns, and C. L. Peterson, 2017 Mechanisms of action and regulation of ATP-dependent chromatin-remodelling complexes. Nat. Rev. Mol. Cell Biol. 18: 407–422. https://doi.org/10.1038/nrm.2017.26

Colot, H. V., G. Park, G. E. Turner, C. Ringelberg, C. M. Crew *et al.*, 2006 A high-throughput gene knockout procedure for Neurospora reveals functions for multiple transcription factors. Proc. Natl. Acad. Sci. USA 103: 10352–10357 (erratum: Proc. Natl. Acad. Sci. USA 103: 16614). https://doi.org/10.1073/pnas.0601456103

Connolly, L. R., K. M. Smith, and M. Freitag, 2013 The *Fusarium graminearum* histone H3 K27 methyltransferase KMT6 regulates development and expression of secondary metabolite gene clusters. PLoS Genet. 9: e1003916. https://doi.org/10.1371/journal.pgen.1003916

Danecek, P., A. Auton, G. Abecasis, C. A. Albers, E. Banks *et al.*, 2011 The variant call format and VCFtools. Bioinformatics 27: 2156–2158. https://doi.org/10.1093/bioinformatics/btr330

Dang, Y., J. Cheng, X. Sun, Z. Zhou, and Y. Liu, 2016 Antisense transcription licenses nascent transcripts to mediate transcriptional gene silencing. Genes Dev. 30: 2417–2432. https://doi.org/10.1101/gad.285791.116

Davis, R. H., 2000 *Neurospora: Contributions of a Model Organism*. Oxford University Press, Oxford.

de Hoon, M. J. L., S. Imoto, J. Nolan, and S. Miyano, 2004 Open source clustering software. Bioinformatics 20: 1453–1454. https://doi.org/10.1093/bioinformatics/bth078

Elgin, S. C. R., and G. Reuter, 2013 Position-effect variegation, heterochromatin formation, and gene silencing in Drosophila. Cold Spring Harb. Perspect. Biol. 5: a017780. https://doi.org/10.1101/cshperspect.a017780

Felle, M., H. Hoffmeister, J. Rothammer, A. Fuchs, J. H. Exler *et al.*, 2011 Nucleosomes protect DNA from DNA methylation *in vivo* and *in vitro*. Nucleic Acids Res. 39: 6956–6969. https://doi.org/10.1093/nar/gkr263

Fillingham, J., P. Kainth, J.-P. Lambert, H. van Bakel, K. Tsui *et al.*, 2009 Two-color cell array screen reveals interdependent roles for histone chaperones and a chromatin boundary regulator in histone gene repression. Mol. Cell 35: 340–351. https://doi.org/10.1016/j.molcel.2009.06.023

Foss, H. M., C. J. Roberts, K. M. Claeys, and E. U. Selker, 1993 Abnormal chromosome behavior in Neurospora mutants defective in DNA methylation. Science 262: 1737–1741. https://doi.org/10.1126/science.7505062

Foss, H. M., C. J. Roberts, and E. U. Selker, 1998 Mutations in the *dim-1* gene of *Neurospora crassa* reduce the level of DNA methylation. Mol. Gen. Genet. 259: 60–71. https://doi.org/10.1007/s004380050789

Freitag, M., 2017 Histone methylation by SET domain proteins in fungi. Annu. Rev. Microbiol. 71: 413–439. https://doi.org/10.1146/annurev-micro-102215-095757

Freitag, M., P. C. Hickey, T. K. Khlafallah, N. D. Read, and E. U. Selker, 2004 HP1 is essential for DNA methylation in Neuros-

pora. Mol. Cell 13: 427–434. https://doi.org/10.1016/S1097-2765(04)00024-3

Gal, C., H. E. Murton, L. Subramanian, A. J. Whale, K. M. Moore *et al.*, 2015 Abo1, a conserved bromodomain AAA-ATPase, maintains global nucleosome occupancy and organisation. EMBO Rep. 17: 79–93. https://doi.org/10.15252/embr.201540476

Galazka, J. M., A. D. Klocko, M. Uesaka, S. Honda, E. U. Selker *et al.*, 2016 Neurospora chromosomes are organized by blocks of importin alpha-dependent heterochromatin that are largely independent of H3K9me3. Genome Res. 26: 1069–1080. https://doi.org/10.1101/gr.203182.115

Gradolatto, A., R. S. Rogers, H. Lavender, S. D. Taverna, C. D. Allis *et al.*, 2008 *Saccharomyces cerevisiae* Yta7 regulates histone gene expression. Genetics 179: 291–304. https://doi.org/10.1534/genetics.107.086520

Grewal, S. I. S., and S. Jia, 2007 Heterochromatin revisited. Nat. Rev. Genet. 8: 35–46. https://doi.org/10.1038/nrg2008

Grossniklaus, U., and R. Paro, 2014 Transcriptional silencing by polycomb-group proteins. Cold Spring Harb. Perspect. Biol. 6: a019331. https://doi.org/10.1101/cshperspect.a019331

Hammond, C. M., C. B. Strømme, H. Huang, D. J. Patel, and A. Groth, 2017 Histone chaperone networks shaping chromatin function. Nat. Rev. Mol. Cell Biol. 18: 141–158. https://doi.org/10.1038/nrm.2016.159

Heard, E., 2005 Delving into the diversity of facultative heterochromatin: the epigenetics of the inactive X chromosome. Curr. Opin. Genet. Dev. 15: 482–489. https://doi.org/10.1016/j.gde.2005.08.009

Henikoff, S., 2000 Heterochromatin function in complex genomes. Biochim. Biophys. Acta 1470: O1–O8.

Henikoff, S., 2016 Mechanisms of nucleosome dynamics *in vivo*. Cold Spring Harb. Perspect. Med. 6: a026666. https://doi.org/10.1101/cshperspect.a026666

Honda, S., and E. U. Selker, 2008 Direct interaction between DNA methyltransferase DIM-2 and HP1 is required for DNA methylation in *Neurospora crassa*. Mol. Cell. Biol. 28: 6044–6055. https://doi.org/10.1128/MCB.00823-08

Honda, S., and E. U. Selker, 2009 Tools for fungal proteomics: multifunctional Neurospora vectors for gene replacement, protein expression and protein purification. Genetics 182: 11–23. https://doi.org/10.1534/genetics.108.098707

Honda, S., Z. A. Lewis, M. Huarte, L. Y. Cho, L. L. David *et al.*, 2010 The DMM complex prevents spreading of DNA methylation from transposons to nearby genes in *Neurospora crassa*. Genes Dev. 24: 443–454. https://doi.org/10.1101/gad.1893210

Honda, S., Z. A. Lewis, K. Shimada, W. Fischle, R. Sack *et al.*, 2012 Heterochromatin protein 1 forms distinct complexes to direct histone deacetylation and DNA methylation. Nat. Struct. Mol. Biol. 19: 471–477. https://doi.org/10.1038/nsmb.2274

Honda, S., V. T. Bicocca, J. D. Gessaman, M. R. Rountree, E. Y. Yu *et al.*, 2016 Dual chromatin recognition by the histone deacetylase complex HCHC is required for proper DNA methylation in *Neurospora crassa*. Proc. Natl. Acad. Sci. USA 113: E6135–E6144 [corrigenda: Proc. Natl. Acad. Sci. USA 114: E1037 (2017)]. https://doi.org/10.1073/pnas.1614279113

Huff, J. T., and D. Zilberman, 2014 Dnmt1-independent CG methylation contributes to nucleosome positioning in diverse eukaryotes. Cell 156: 1286–1297. https://doi.org/10.1016/j.cell.2014.01.029

Iyer, V., and K. Struhl, 1995 Poly(dA:dT), a ubiquitous promoter element that stimulates transcription via its intrinsic DNA structure. EMBO J. 14: 2570–2579. https://doi.org/10.1002/j.1460-2075.1995.tb07255.x

Jamieson, K., M. R. Rountree, Z. A. Lewis, J. E. Stajich, and E. U. Selker, 2013 Regional control of histone H3 lysine 27 methylation in Neurospora. Proc. Natl. Acad. Sci. USA 110: 6027–6032. https://doi.org/10.1073/pnas.1303750110

Jamieson, K., E. T. Wiles, K. J. McNaught, S. Sidoli, N. Leggett *et al.*, 2016 Loss of HP1 causes depletion of H3K27me3 from facultative heterochromatin and gain of H3K27me2 at constitutive heterochromatin. Genome Res. 26: 97–107. https://doi.org/10.1101/gr.194555.115

Kalashnikova, E. V., A. S. Revenko, A. T. Gemo, N. P. Andrews, C. G. Tepper *et al.*, 2010 ANCCA/ATAD2 overexpression identifies breast cancer patients with poor prognosis, acting to drive proliferation and survival of triple-negative cells through control of B-Myb and EZH2. Cancer Res. 70: 9402–9412. https://doi.org/10.1158/0008-5472.CAN-10-1199

Kent, N. A., S. Adams, A. Moorhouse, and K. Paszkiewicz, 2010 Chromatin particle spectrum analysis: a method for comparative chromatin structure analysis using paired-end mode next-generation DNA sequencing. Nucleic Acids Res. 39: e26. https://doi.org/10.1093/nar/gkq1183

Klocko, A. D., M. R. Rountree, P. L. Grisafi, S. M. Hays, K. K. Adhvaryu *et al.*, 2015 Neurospora importin α is required for normal heterochromatic formation and DNA methylation. PLoS Genet. 11: e1005083. https://doi.org/10.1371/journal.pgen.1005083

Klocko, A. D., T. Ormsby, J. M. Galazka, N. A. Leggett, M. Uesaka *et al.*, 2016 Normal chromosome conformation depends on subtelomeric facultative heterochromatin in *Neurospora crassa*. Proc. Natl. Acad. Sci. USA 113: 15048–15053. https://doi.org/10.1073/pnas.1615546113

Krietenstein, N., M. Wal, S. Watanabe, B. Park, C. L. Peterson *et al.*, 2016 Genomic nucleosome organization reconstituted with pure proteins. Cell 167: 709–721.e12. https://doi.org/10.1016/j.cell.2016.09.045

Lai, W. K. M., and B. F. Pugh, 2017 Understanding nucleosome dynamics and their links to gene expression and DNA replication. Nat. Rev. Mol. Cell Biol. 18: 548–562. https://doi.org/10.1038/nrm.2017.47

Lämke, J., and I. Bäurle, 2017 Epigenetic and chromatin-based mechanisms in environmental stress adaptation and stress memory in plants. Genome Biol. 18: 124. https://doi.org/10.1186/s13059-017-1263-6

Langmead, B., and S. L. Salzberg, 2012 Fast gapped-read alignment with Bowtie 2. Nat. Methods 9: 357–359. https://doi.org/10.1038/nmeth.1923

Lee, H.-C., L. Li, W. Gu, Z. Xue, S. K. Crosthwaite *et al.*, 2010 Diverse pathways generate microRNA-like RNAs and Dicer-independent small interfering RNAs in fungi. Mol. Cell 38: 803–814. https://doi.org/10.1016/j.molcel.2010.04.005

Lewis, P. W., and C. D. Allis, 2013 Poisoning the "histone code" in pediatric gliomagenesis. Cell Cycle 12: 3241–3242. https://doi.org/10.4161/cc.26356

Lewis, P. W., M. M. Müller, M. S. Koletsky, F. Cordero, S. Lin *et al.*, 2013 Inhibition of PRC2 activity by a gain-of-function H3 mutation found in pediatric glioblastoma. Science 340: 857–861. https://doi.org/10.1126/science.1232245

Lewis, Z. A., S. Honda, T. K. Khlafallah, J. K. Jeffress, M. Freitag *et al.*, 2008 Relics of repeat-induced point mutation direct heterochromatin formation in *Neurospora crassa*. Genome Res. 19: 427–437. https://doi.org/10.1101/gr.086231.108

Lewis, Z. A., K. K. Adhvaryu, S. Honda, A. L. Shiver, M. Knip *et al.*, 2010a DNA methylation and normal chromosome behavior in Neurospora depend on five components of a histone methyltransferase complex, DCDC. PLoS Genet. 6: e1001196. https://doi.org/10.1371/journal.pgen.1001196

Lewis, Z. A., K. K. Adhvaryu, S. Honda, A. L. Shiver, and E. U. Selker, 2010b Identification of DIM-7, a protein required to target the DIM-5 H3 methyltransferase to chromatin. Proc. Natl. Acad. Sci. USA 107: 8310–8315. https://doi.org/10.1073/pnas.1000328107

Liu, J., W. Lee, Z. Jiang, Z. Chen, S. Jhunjhunwala *et al.*, 2012 Genome and transcriptome sequencing of lung cancers

reveal diverse mutational and splicing events. Genome Res. 22: 2315–2327. https://doi.org/10.1101/gr.140988.112

Lombardi, L. M., A. Ellahi, and J. Rine, 2011 Direct regulation of nucleosome density by the conserved AAA-ATPase Yta7. Proc. Natl. Acad. Sci. USA 108: E1302–E1311. https://doi.org/10.1073/pnas.1116819108

Lombardi, L. M., M. D. Davis, and J. Rine, 2014 Maintenance of nucleosomal balance in cis by conserved AAA-ATPase Yta7. Genetics 199: 105–116. https://doi.org/10.1534/genetics.114.168039

Miao, V. P., M. Freitag, and E. U. Selker, 2000 Short TpA-rich segments of the ζ-η region induce DNA methylation in *Neurospora crassa*. J. Mol. Biol. 300: 249–273. https://doi.org/10.1006/jmbi.2000.3864

Morgan, M. A., and A. Shilatifard, 2015 Chromatin signatures of cancer. Genes Dev. 29: 238–249. https://doi.org/10.1101/gad.255182.114

Nielsen, P. R., D. Nietlispach, H. R. Mott, J. Callaghan, A. Bannister *et al.*, 2002 Structure of the HP1 chromodomain bound to histone H3 methylated at lysine 9. Nature 416: 103–107. https://doi.org/10.1038/nature722

Okano, M., D. W. Bell, D. A. Haber, and E. Li, 1999 DNA methyltransferases Dnmt3a and Dnmt3b are essential for *de novo* methylation and mammalian development. Cell 99: 247–257. https://doi.org/10.1016/S0092-8674(00)81656-6

Quintales, L., E. Vázquez, and F. Antequera, 2014 Comparative analysis of methods for genome-wide nucleosome cartography. Brief. Bioinform. 16: 576–587. https://doi.org/10.1093/bib/bbu037

Ramírez, F., D. P. Ryan, B. Grüning, V. Bhardwaj, F. Kilpert *et al.*, 2016 deepTools2: a next generation web server for deep-sequencing data analysis. Nucleic Acids Res. 44: W160–W165. https://doi.org/10.1093/nar/gkw257

Revenko, A. S., E. V. Kalashnikova, A. T. Gemo, J. X. Zou, and H.-W. Chen, 2010 Chromatin loading of E2F-MLL complex by cancer-associated coregulator ANCCA via reading a specific histone mark. Mol. Cell. Biol. 30: 5260–5272. https://doi.org/10.1128/MCB.00484-10

Roberts, C. J., and E. U. Selker, 1995 Mutations affecting the biosynthesis of S-adenosylmethionine cause reduction of DNA methylation in *Neurospora crassa*. Nucleic Acids Res. 23: 4818–4826. https://doi.org/10.1093/nar/23.23.4818

Robinson, J. T., H. Thorvaldsdóttir, W. Winckler, M. Guttman, E. S. Lander *et al.*, 2011 Integrative genomics viewer. Nat. Biotechnol. 29: 24–26. https://doi.org/10.1038/nbt.1754

Ronemus, M. J., M. Galbiati, C. Ticknor, J. Chen, and S. L. Dellaporta, 1996 Demethylation-induced developmental pleiotropy in Arabidopsis. Science 273: 654–657. https://doi.org/10.1126/science.273.5275.654

Rountree, M. R., and E. U. Selker, 2010 DNA methylation and the formation of heterochromatin in *Neurospora crassa*. Heredity 105: 38–44. https://doi.org/10.1038/hdy.2010.44

Saldanha, A. J., 2004 Java Treeview–extensible visualization of microarray data. Bioinformatics 20: 3246–3248. https://doi.org/10.1093/bioinformatics/bth349

Segal, E., and J. Widom, 2009 Poly(dA:dT) tracts: major determinants of nucleosome organization. Curr. Opin. Struct. Biol. 19: 65–71. https://doi.org/10.1016/j.sbi.2009.01.004

Selker, E. U., N. A. Tountas, S. H. Cross, B. S. Margolin, J. G. Murphy *et al.*, 2003 The methylated component of the *Neurospora crassa* genome. Nature 422: 893–897. https://doi.org/10.1038/nature01564

Seymour, M., L. Ji, A. M. Santos, M. Kamei, T. Sasaki *et al.*, 2016 Histone H1 limits DNA methylation in *Neurospora crassa*. G3 (Bethesda) 6: 1879–1889. https://doi.org/10.1534/g3.116.028324

Soppe, W. J. J., Z. Jasencakova, A. Houben, T. Kakutani, A. Meister *et al.*, 2002 DNA methylation controls histone H3 lysine 9 methylation and heterochromatin assembly in Arabidopsis. EMBO J. 21: 6549–6559. https://doi.org/10.1093/emboj/cdf657

Studt, L., S. M. Rösler, I. Burkhardt, B. Arndt, M. Freitag *et al.*, 2016 Knock-down of the methyltransferase Kmt6 relieves H3K27me3 and results in induction of cryptic and otherwise silent secondary metabolite gene clusters in *Fusarium fujikuroi*. Environ. Microbiol. 18: 4037–4054. https://doi.org/10.1111/1462-2920.13427

Sun, F. L., M. H. Cuaycong, and S. C. Elgin, 2001 Long-range nucleosome ordering is associated with gene silencing in *Drosophila melanogaster* pericentric heterochromatin. Mol. Cell. Biol. 21: 2867–2879. https://doi.org/10.1128/MCB.21.8.2867-2879.2001

Tachibana, M., K. Sugimoto, M. Nozaki, J. Ueda, T. Ohta *et al.*, 2002 G9a histone methyltransferase plays a dominant role in euchromatic histone H3 lysine 9 methylation and is essential for early embryogenesis. Genes Dev. 16: 1779–1791. https://doi.org/10.1101/gad.989402

Takeshima, H., I. Suetake, and S. Tajima, 2008 Mouse Dnmt3a preferentially methylates linker DNA and is inhibited by histone H1. J. Mol. Biol. 383: 810–821. https://doi.org/10.1016/j.jmb.2008.03.001

Timp, W., and A. P. Feinberg, 2013 Cancer as a dysregulated epigenome allowing cellular growth advantage at the expense of the host. Nat. Rev. Cancer 13: 497–510. https://doi.org/10.1038/nrc3486

Trojer, P., and D. Reinberg, 2007 Facultative heterochromatin: is there a distinctive molecular signature? Mol. Cell 28: 1–13. https://doi.org/10.1016/j.molcel.2007.09.011

Tsukiyama, T., 2002 The *in vivo* functions of ATP-dependent chromatin-remodelling factors. Nat. Rev. Mol. Cell Biol. 3: 422–429. https://doi.org/10.1038/nrm828

Vermaak, D., and A. P. Wolffe, 1998 Chromatin and chromosomal controls in development. Dev. Genet. 22: 1–6. https://doi.org/10.1002/(SICI)1520-6408(1998)22:1<1::AID-DVG1>3.0.CO;2-A

Vogel, M. J., D. Peric-Hupkes, and B. van Steensel, 2007 Detection of *in vivo* protein-DNA interactions using DamID in mammalian cells. Nat. Protoc. 2: 1467–1478. https://doi.org/10.1038/nprot.2007.148

Wiles, E. T., and E. U. Selker, 2017 H3K27 methylation: a promiscuous repressive chromatin mark. Curr. Opin. Genet. Dev. 43: 31–37. https://doi.org/10.1016/j.gde.2016.11.001

Wutz, A., 2011 Gene silencing in X-chromosome inactivation: advances in understanding facultative heterochromatin formation. Nat. Rev. Genet. 12: 542–553. https://doi.org/10.1038/nrg3035

Xu, S., S. Grullon, K. Ge, and W. Peng, 2014 Spatial clustering for identification of ChIP-enriched regions (SICER) to map regions of histone methylation patterns in embryonic stem cells. Methods Mol. Biol. 1150: 97–111. https://doi.org/10.1007/978-1-4939-0512-6_5

Zhang, Y., T. Liu, C. A. Meyer, J. Eeckhoute, D. S. Johnson *et al.*, 2008 Model-based analysis of ChIP-seq (MACS). Genome Biol. 9: R137. https://doi.org/10.1186/gb-2008-9-9-r137

Zou, J. X., A. S. Revenko, L. B. Li, A. T. Gemo, and H.-W. Chen, 2007 ANCCA, an estrogen-regulated AAA+ ATPase coactivator for ERalpha, is required for coregulator occupancy and chromatin modification. Proc. Natl. Acad. Sci. USA 104: 18067–18072. https://doi.org/10.1073/pnas.0705814104

Zou, J. X., L. Guo, A. S. Revenko, C. G. Tepper, A. T. Gemo *et al.*, 2009 Androgen-induced coactivator ANCCA mediates specific androgen receptor signaling in prostate cancer. Cancer Res. 69: 3339–3346. https://doi.org/10.1158/0008-5472.CAN-08-3440

Communicating editor: O. Rando